Supporting Information

Mukherjee and Warshel 10.1073/pnas.1317641110

I. General Considerations

Despite the immense progress in understanding the overall myosin V cycle from structural, kinetics, and single-molecule experiments, a quantitative knowledge of the structure/energy relationship behind the unidirectionality of the myosin V processive cycle is still lacking. The primary challenge that one encounters is to combine the biochemical and structural findings in a well-defined physical model that reproduces the observed directionality without the need to model it through phenomenological parameters. To advance toward any kind of structure-based understanding of the unidirectional motion in myosin, one must obtain a clear concept of the underlying free energy surface. Here, we illustrate the different possibilities that can lead to an overall bias toward the forward motion of myosin V on actin filaments (right indicates the "plus end") in Fig. S1. Considering the free energy surface of the whole process, we have only two options for a net directional motion to the right. Either the free energy goes up on the left direction (analogous to a thermodynamically controlled mechanism) or the barrier to the left direction is higher than that to the right (analogous to a kinetically controlled mechanism). In the second case the free energy of the left motion can be as low as that of the right motion. Here, the use of arguments like "diffusive motion" or on "futile lever arm swings" (1) are much less relevant in understanding the function, especially when the focus is to obtain a clear quantitative argument of the directionality issue. Constructing such a model based on structural and kinetics observations should provide an understanding of the coupling between the large lever arm movement (repriming and powerstroke) and the catalytic or actin binding/release cycles.

In considering the tentative reasons that can give rise to the directionality, we should focus on the asymmetric elements in the system. There are several ways of introducing structural asymmetry in the myosin V molecule as it walks over actin filament, but the most obvious among them are the asymmetry in the interactions arising due to θ_{up} and θ_{down} conformations, the asymmetry generated in the upper fork where two lever arms meet, asymmetry generated in the leading and lagging lever arms while walking, and asymmetry in the interaction of myosin heads with the actin filament. The asymmetry in the contacts between the myosin and actin is in principle possible but is inconsistent with the finding of similar binding modes and interactions for both heads. Furthermore, the asymmetry in the fork region or the geometry of long lever arms are also unlikely to contribute to the overall free energy driving the directional motion, because the final configurations in the left and right ends of a single cycle are identical (Fig. S1). Thus, in this study, we will focus on understanding how the structural changes in the lever arm during powerstroke or repriming is coupled to the other chemical events of the cycle and how this coupling might help propagating the directional motion.

II. Structural Considerations for the Myosin V Model

The high-resolution structures of the lever arm for the prepowerstroke state is not available for myosin V, although the same is available for myosin II, which shares a high structural conservation with myosin V (2). Moreover, we are interested in models of myosin V structures with parts of the lever arm lying adjacent to the head domain (with two bound calmodulins out of six) and thus can use the information of truncated myosin II lever positions to model them. A detailed study of the θ_{up} and θ_{down} structural states of myosin II has revealed the distinct conformation that the lever arm and convertor domain adopts during the swinging movement along with the kink in the relay helix (3). In order to model the lever arm and convertor domain/relay helix position in the pre- and postpowerstroke states, we have used myosin II structures (1QVI for pre- or θ_{up} conformation and 1SR6 for post- or θ_{down} conformation) to model the similar conformations for myosin V with SWISS-MODEL (http://swissmodel.expasy.org/). Furthermore, the two θ_{up} and θ_{down} structures of modeled myosin V were superimposed using the actin- and nucleotide-binding domains and a common axis (tentatively perpendicular to the actin binding surface) was generated using the convertor domain and the base of the lever arm. This axis was used to rotate the lever arm of the myosin V to produce θ_{up} and θ_{down} values (shown in Fig. 2*B*). It should be noted that the angular θ values just provide an estimate of the progression of the conformational reaction coordinate and bear no real significance to the actual results. The relative free energy of the conformations, rather than the angular θ value, was used to model the mechanochemical cycle presented in Figs. 4 and 5 of the main text. Intermediate structures between the myosin V θ_{up} and θ_{down} conformations were generated using a linear interpolation scheme and each of the structures was relaxed to relieve short contacts of the coarse-grained (CG) side chains. The CG free energy profile is shown and discussed in the main text (Fig. 2*B*), and we also provide in Fig. S2 the contributions from residues that are most affected (more than 1 kcal change in relative free energy) during the conformational change of the lever arm-swing movement. The figure shows that the most affected residues are clustered around the part of the relay helix (shown in yellow) close to the convertor domain. It is found that some residues on the convertor domain and the base of the lever arm are affected drastically. The most affected charged residues are 73D, 82E, and 689E lying close to the convertor domain; 473E, 476E, and 479K of the relay helix; 748K of the convertor domain; and E760 at the base of the lever arm. It should be noted that the polar and nonpolar groups could also have an indirect impact on the contributions of ionized residues to the free energy change. A more detailed analysis of the residue-specific contributions should try to correlate the available experimental mutations in other myosin structures (such as myosin II, myosin V, myosin I, etc.) to arrive at a consensus model regarding the role of specific residues in the mechanochemical coupling in myosin motors.

III. Energetics of the Chemical Steps of Single-Headed Myosin V

One of the most important elements of quantifying the action of myosin is the conversion of the available kinetic and thermodynamic information on the single-headed myosin V to their relevant energetics. This is done in Table S2 and a surface representation of the energetics is presented in Fig. S3. The free energies/barriers calculated using basic principles of chemical rate equations are used as an important element in the analysis of the myosin V motion discussed in the main text.

IV. Additional Information About the Energetics of Myosin V

Owing to space limitations we provide some of our analysis about myosin V walking cycle in *Supporting Information*. In particular, we show our calculations of the energetics involved in the reverse motion of myosin V on actin filaments in Fig. S4. The figure is similar to Fig. 4 in the main text, except for the fact that it represents the motion of myosin V in the nonfunctional direction. The resulting one-dimensional energy profile of the nonfunctional motion is, however, shown and discussed in the main text (Fig. 5*B*).

V. The CG Model Used to Generate the Electrostatic Free Energy Surface of the Conformational Transition

The present work uses a CG model that describes the main chains by an explicit all-atom model and represents the side chains as a simplified united atom model. This CG model provides a more advanced treatment of electrostatic effect than most current CG models. More specifically, the present model is a slightly modified version of our recent work (4, 5) and expresses the overall free energy as

$$\Delta G_{total} = \Delta G_{main} + \Delta G_{main-side} + \Delta G_{side}. \quad \textbf{[S1]}$$

The all-atom main chain is treated with implicit solvent corrections, and the main-side treatment involves van der Waals and screened electrostatic terms (5). The major and most relevant part of our treatment comes from the ΔG_{side}, which is given by

$$\Delta G_{side} = \Delta G^{vdw}_{side} + \Delta G^{elec}_{side} + \Delta G_{hyd}. \quad \textbf{[S2]}$$

The first term describes the effective van der Waals interactions between simplified side chains, which is described in ref. 5. The second term represents the electrostatic energy of the ionizable residues (discussed below), and the last term represents the hydrophobic contributions, which are not included implicitly in the first term (see ref. 6 for a discussion of the hydrophobic terms).

The ΔG^{elec}_{side} term is given by

$$\Delta G^{elec}_{side} = -2.3RT\sum_i Q_i\left(pK^w_{a,i} - pH\right) + \Delta G_{QQ} + \Delta G_{self}, \quad \textbf{[S3]}$$

where i runs over the protein ionizable residues and the proton placed inside the protein, $pK^w_{a,i}$ is the pK^a of the i^{th} residue in water, and Q_i is the charge of the i^{th} residue in the given ionization state. ΔG_{QQ} is the charge–charge interaction free energy, which is given by

$$\Delta G_{QQ} = \frac{\sum_i \sum_{j\neq i} 166 Q_i Q_j}{r_{ij}\varepsilon_{eff}}, \quad \textbf{[S4]}$$

where the energy is given in kilocalories per mole and the distances in angstroms. ε_{eff} is the effective dielectric for charge–charge interaction, which reflects the idea established in many of our works (e.g., refs. 5–8), that the optimal value is large even in protein interiors (namely, $\varepsilon_{eff} > 20$). This type of dielectric has been found recently to provide very powerful insight in studies of protein stability (see refs. 7 and 8) and thus it is expected to be very useful in modeling the electrostatic contribution to the stability of the simplified model. The ionization state of the protein residues were determined by the Monte Carlo approach of ref. 5 for the assumed pH of 7.

A key element in our approach is the treatment of the self-energy, ΔG_{self}, associated with charging each ionized group in its specific environment. This term is described in detail in ref. 5. Additional key features and more recent refinements of the treatment of the protein and the membrane system are described in the supporting information of ref. 9.

All of the above electrostatic treatment involves a self-consistent treatment of the interdependent self-energy, charge–charge interaction and the external pH (where the ionization state is determined by a Monte Carlo treatment of the energetics of Eq. **S3**).

1. Málnási-Csizmadia A, Kovács M (2010) Emerging complex pathways of the actomyosin powerstroke. *Trends Biochem Sci* 35(12):684–690.
2. Sweeney HL, Houdusse A (2010) Structural and functional insights into the myosin motor mechanism. *Annu Rev Biophys* 39:539–557.
3. Houdusse A, Szent-Gyorgyi AG, Cohen C (2000) Three conformational states of scallop myosin S1. *Proc Natl Acad Sci USA* 97(21):11238–11243.
4. Dryga A, Chakrabarty S, Vicatos S, Warshel A (2011) Coarse grained model for exploring voltage dependent ion channels. *Biochim Biophys Acta* 1818(2):303–317.
5. Messer BM, et al. (2010) Multiscale simulations of protein landscapes: Using coarse-grained models as reference potentials to full explicit models. *Proteins* 78(5):1212–1227.
6. Rychkova A, Warshel A (2013) Exploring the nature of the translocon-assisted protein insertion. *Proc Natl Acad Sci USA* 110:495–500.
7. Roca M, Messer B, Warshel A (2007) Electrostatic contributions to protein stability and folding energy. *FEBS Lett* 581(10):2065–2071.
8. Warshel A, Sharma PK, Kato M, Parson WW (2006) Modeling electrostatic effects in proteins. *Biochim Biophys Acta* 1764(11):1647–1676.
9. Dryga A, Chakrabarty S, Vicatos S, Warshel A (2012) Realistic simulation of the activation of voltage-gated ion channels. *Proc Natl Acad Sci USA* 109(9):3335–3340.

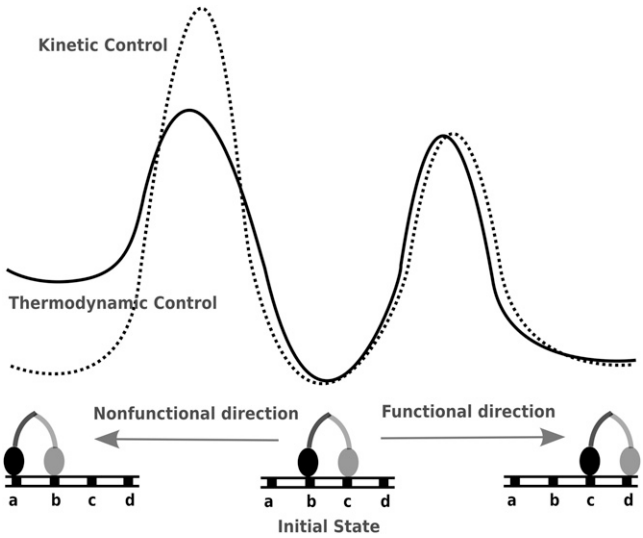

Fig. S1. Tentative conditions responsible for the directionality of myosin V stepping over the actin filaments are schematically shown. The options of thermodynamic control (adopting a pathway that reduces the overall free energy in the correct functional direction) and kinetic control (adopting a pathway that has lower effective barriers for moving in the correct functional direction) are the two possibilities underlying the movement of myosin V in the functional direction.

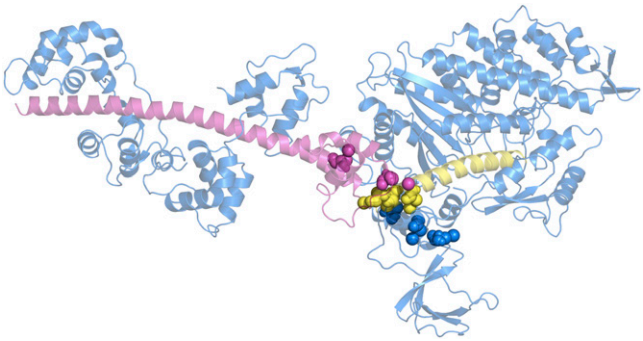

Fig. S2. Structure of myosin V is shown. The lever arm and the convertor domain is in magenta, the relay helix is in yellow, and the rest of the protein is in blue. The residues showing the highest free energy changes (more than 1 kcal) between the pre- and postpowerstroke states are highlighted in spheres.

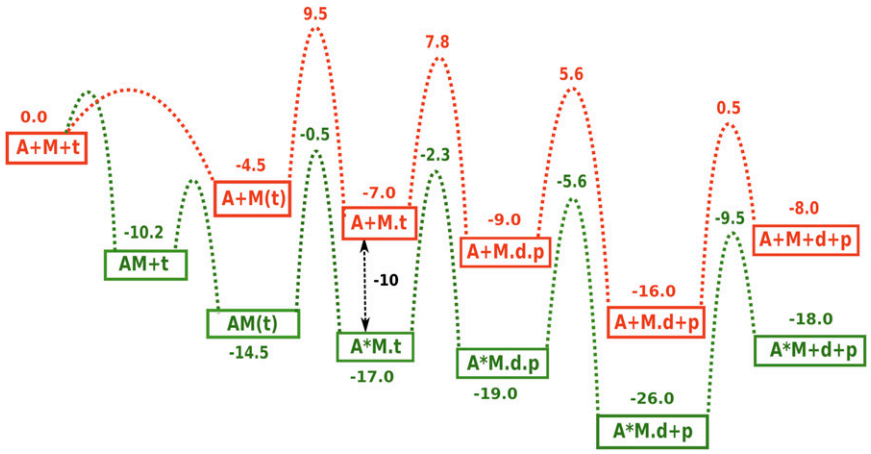

Fig. S3. A one-dimensional free energy surface for moving along the chemical steps along the functional path of myosin V is shown. The surface is based on the analysis of the experimental kinetics and thermodynamics provided in Table S2. The red path shows the kinetics for the actin-free single-headed strand of myosin V molecule, and the green path shows the same for the actin-bound single-headed strand of myosin V. Note that the difference between the actin-free and -bound states is around 10 kcal.

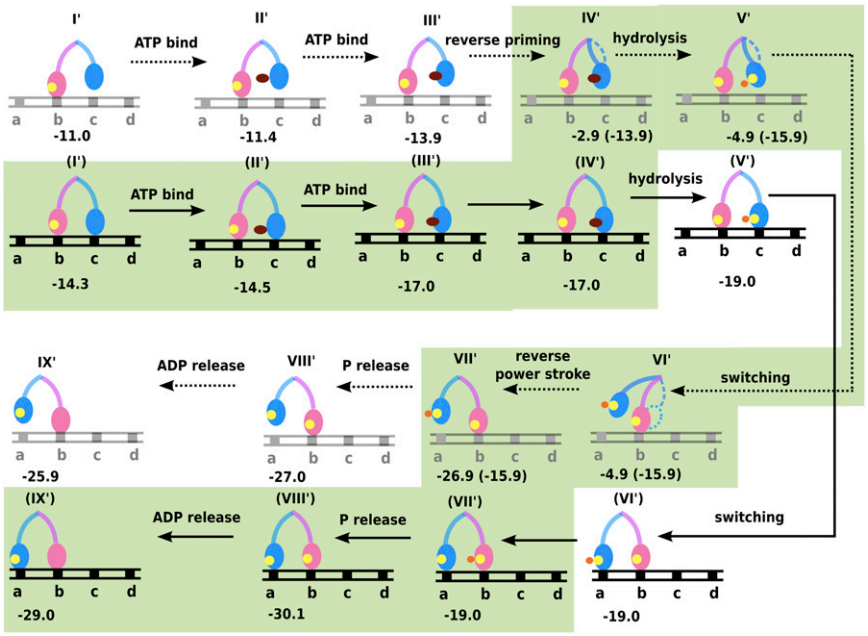

Fig. S4. The free energy landscape (obtained by combining the information from Figs. 2 and 3) for myosin V walking toward the opposite direction is shown. Above, states denoted I′ to IX′ is when myosin V lagging strand (pink) is in the actin-free state, and below states denoted in (I′) to (IX′) are for both myosin V strands bound to actin. The nucleotide occupancies are denoted in deep red, yellow, and orange spheres for ATP, ADP, and P_i, respectively. The actin is shown as a black or gray track with equally spaced myosin binding sites denoted as a, b, c, and d, where moving in d → a indicates the "minus end" direction. The free energy path highlighted in green reveal a clear uphill path compared with myosin V walking from a → d (Fig. 4 in the main text).

Table S1. The breakup of the total CG energy for the two key myosin V states

Myosin V conformational states	ΔG_{elec}	$\Delta G_{hydrophobic}$	ΔG_{main}	ΔG_{HB}
θ_{up}	−243.37	66.27	−468.29	−19.54
θ_{down}	−232.20	69.76	−467.25	−19.71

The electrostatic (ΔG_{elec}) and hydrophobic contribution ($\Delta G_{hydrophobic}$) for CG side chains and the contributions from the main chain solvation (ΔG_{main}) and backbone H-bonds (ΔG_{HB}) are tabulated.

Table S2. The energetics of single-headed truncated myosin V molecules in different key steps

Steps	ΔG	$\Delta g^{\ddagger}$	Ref.
		ATP binding	
[M + t ↔M(t) t →M.t][†]	−4.59	≤14.0	1
	?	?	2
	?	?	3
[AM+t ↔AM(t)→A*M.t][‡]	−4.27	13.9	1
	−4.19	13.8	2
	?	?	3
		Hydrolysis	
[M.t → M.d.p][§]	−1.0	<14.6	1
	?	?	2
	?	14.8	3
[AM.t → AM.d.p][¶]	?	<14.6	1
	?	?	2
	?	?	3
		P release	
[M.d.p → M.d][‖]	? (Irreversible)	<14.6	1
	?	?	2
	?	?	3
[AM.d.p → AM.d] **	?	?	None
		ADP release (rate-limiting step)	
[M.d → M + d] [††]	9.07	d dissociation: 16.5	1
	?	?	2
	8.08	d dissociation: 16.5	3
[AM.d → AM + d] [‡‡]	8.33	d dissociation: 16.4	1
	?	Steady-state rate: 16.5	2
	7.87	d dissociation: 16.4	3
		Actin release from M.d	
[AM.d → A + M.d] [§§]	11.2	Dissociation: 20.0	1
	?	?	2
	9.96	?	3
[AM.t → A + M.t] [¶¶]	9.25	?	2
[A*M.t → A + M.t] [¶¶]	7.87–7.45	?	2
[A*M*t → A + M*t] [¶¶]	≤6.9	?	2
		Actin binding to myosin	
[A+ M + t → AM + t]***	−15.5	?	1
[A+ M + d → AM + d]***	?	?	2
[A + M → AM]***	−10.17	?	3

Energies in kilocalories per mole. A, M, t, d, and p designate, respectively, actin, myosin, ATP, ADP, and inorganic phosphate. The sources of the different energies are given in the last column.

[†]The binding of t is denoted by [M + t ↔ M(t) →M.t]. Here the equilibrium step is determined by K_1 and the second step by a rate constant k_2. The ΔG and $\Delta g^{\ddagger}$ are calculated from $K_1k_2 = 1.6\ \mu M^{-1}s^{-1}$ and $k_2 \geq 750\ s^{-1}$ in ref. 1. Refs. 2 and 3 give the values of $K_1k_2 = 1.6\ \mu M^{-1}\cdot s^{-1}$ and $7 \times 10^5\ M^{-1}\cdot s^{-1}$, respectively, which are similar to ref. 1.

[‡]The binding of t is denoted by [AM + t ↔ AM(t) →A*M.t] (scheme 3 of ref. 2). Here the equilibrium step is determined by K_1' and the second step by a rate constant k_2'. The ΔG are calculated from $K_1' = 815\ \mu M$ and 925 μM in refs. 1 and 2, respectively. The $\Delta g^{\ddagger}$ are calculated from $k_2' = 870\ s^{-1}$ and $899\ s^{-1}$ in refs. 1 and 2, respectively; ref. 3. gives the value of $K_1'k_2' = 7 \times 10^5\ M^{-1}\cdot s^{-1}$, which is similar to others.

[§]The hydrolysis is denoted by [M.t ↔ M.d.p]. The ΔG is calculated from $K_3 = 5.3$, which is taken from ref. 1. The higher limit of $\Delta g^{\ddagger}$ are calculated from $k_{+3} + k_{-3} \geq 250\ s^{-1}$ and $k_{+3} + k_{-3} = 200\ s^{-1}$ in refs. 1 and 3, respectively.

[¶]The hydrolysis is denoted by [AM.t ↔ AM.d.p]. This value is thought to be similar to that in [§](i.e., $k_{+3} + k_{-3} = k_{+3}' + k_{-3}'$) in ref. 1.

[‖]The phosphate release is denoted by [M.d.p ↔ M.d]. De La Cruz et al. (1) remark that both hydrolysis and P_i release rates are $>250\ s^{-1}$. It is also noted that the P_i release step is irreversible.

**The phosphate release is denoted by [AM.d.p ↔ AM.d]. None of the studies considered report substantially on this.

[††]The release of d is denoted by [M.d ↔ M + d] and is rate-limiting. ΔG is obtained from the observed dissociation constant, which is reported as 0.27 μM and 1.4 μM in refs. 1 and 3, respectively. The rate of ADP dissociation is reported in the range of 12–16 s^{-1} in both refs. 1 and 3.

[‡‡]The release of d is denoted by [AM.d ↔ AM + d]. ΔG is obtained from the observed dissociation constant, which is reported as 0.93 μM and 2.0 μM in refs. 1 and 3, respectively. The rate of ADP dissociation are reported in the range of 16 s^{-1} in ref. 1 and 13–22 s^{-1} in ref. 3, whereas steady-state rate is reported as 15 s^{-1} in ref. 2.

[§§]The actin release is denoted by [AM.d ↔ A + M.d]. ΔG is obtained from the observed dissociation constant, which is reported as 7.6 nM and 61 nM in refs. 1 and 3. The rate of actin dissociation is reported in the range of 0.032 s^{-1} in ref. 1.

[¶¶]The actin release is denoted by [AM.t ↔ A + M.t], [A*M.t ↔ A + M.t], or [A*M*t ↔ A + M*t] (schemes taken from ref. 2). ΔG is obtained from the observed dissociation constant, which is reported as 0.2 μM, 2–4 μM, and ≥10 μM in ref. 2 for three rate equations, respectively.

***The actin binding is denoted by [A + M↔ AM] or [A + M + t/d↔ AM + t/d]. ΔG is calculated from 4.9×10^{-12} M or 43 nM in refs. 1 and 3, respectively.

1. De La Cruz EM, Wells AL, Rosenfeld SS, Ostap EM, Sweeney HL (1999) The kinetic mechanism of myosin V. *Proc Natl Acad Sci USA* 96(24):13726–13731.
2. Yengo CM, De la Cruz EM, Safer D, Ostap EM, Sweeney HL (2002) Kinetic characterization of the weak binding states of myosin V. *Biochemistry* 41(26):8508–8517.
3. Trybus KM, Krementsova E, Freyzon Y (1999) Kinetic characterization of a monomeric unconventional myosin V construct. *J Biol Chem* 274(39):27448–27456.